RSC Advances

ROYAL SOCIETY OF CHEMISTRY

www.rsc.org/advances

One-step synthesis of cobalt sulfide/reduced graphene oxide composite used as electrode material for supercapacitor

Liang Xu, Yun Lu*

Department of Polymer Science and Engineering, State Key Laboratory of Coordination Chemistry, Collaborative Innovation Center of Chemistry for Life Science, Key Laboratory of High Performance Polymer Materials and Technology of Ministry of Education, School of Chemistry and Chemical Engineering, Nanjing University, Nanjing 210093, China

* Prof. Dr. Yun Lu, Corresponding author

Department of Polymer Science and Engineering, School of Chemistry and Chemical Engineering, Nanjing University, Nanjing 210093, China

E-mail: yunlu@nju.edu.cn

Abstract

A simple, one-step approach has been developed to prepare a composite of cobalt sulfide/reduced graphene oxide (CoS/rGO) by using sodium thiosulfate as a sulfur source. The reduction of GO and the growth of CoS occurred simultaneously, forming a hybrid structure with CoS anchoring on rGO surface. The prepared CoS/rGO composite was applied as an electrode material and found to exhibit a high specific capacitance and rate capability, such as 550 F/g and 400 F/g at a current density of 1 A/g and 40 A/g respectively as well as excellent cyclic stability for 5000 cycles of

charge-discharge. The CoS/rGO composite could be a promising electrode material for a high performance supercapacitor.

Keywords

Cobalt sulfide; Capacitances; Supercapacitor; Electrochemical characterization.

Introduction

The studies on metal sulfides and their specific capacitance have attracted increasing attention [1-4], mainly due to their potential application in electrochemical supercapacitors and lithium-ion batteries. Among them, cobalt sulfides, e.g., Co_9S_8, Co_3S_4, CoS_2, CoS and $Co_{1-x}S$, are unique because of their different crystalline phases and metal valence states, and have been considered as one of the most promising electrode materials [5-10]. However, these valuable materials still have drawbacks, i.e., low conductivity and poor cyclability [11, 12].

Carbon materials, e.g., activated carbon[13], carbon aerogels [14], carbon nanotubes [15], carbon nanofibres [16], templated porous carbon [17] and graphene [18, 19], have also attracted a great deal of interest in recent years because of their extraordinary properties, such as high specific surface area, excellent electric conductivity and flexibility. However, some deficiencies for carbon materials should not be overlooked, such as a high interparticle resistance, a limited specific capacitance, and a low energy density.

To overcome the innate drawbacks of single materials, one of the most intensive approaches is the development of new composite materials, which may not only

improve the performances of each component but also create the new functions owning to the synergic effect originated from recombination. Recently, much effort has been put into the development of metal sulfides-based graphene composites [1, 20-26], in which the synthesis of the composite is usually multi-step and high-cost. In this study, a cobalt sulfides/reduced graphene oxide (CoS/rGO) composite has been synthesized via a simple, one-step hydrothermal method by using $Na_2S_2O_3$ as a sulfur source and hydrazine hydrate as a reductant. The electrochemical tests suggested that the obtained composite exhibited a high rate capability and good cycling stability as used for an electrode of a supercapacitor.

Experimental

Preparation of GO

GO was prepared from graphite powder by a modified Hummers method [27]. Specifically, 6 g of graphite was added into 40 mL of concentrated H_2SO_4, followed by adding 5 g of $K_2S_2O_8$ and 5 g of P_2O_5. The mixture was heated to 80 ℃ and maintained for 24 h. It was then diluted with 250 mL of distilled (DI) water. The product was filtered, washed with DI water for several times, and dried. The obtained pre-oxidized graphite was put into 150 mL of concentrated H_2SO_4 with mechanical stirring, and to which, at the same time, 30 g of $KMnO_4$ powder was slowly added under ice-bath. After being stirred at 35 ℃ for 24 h, the products were transferred into 200 mL of distilled water, then to which 10 mL of 30 % H_2O_2 was added drop by drop. The obtained GO suspension was centrifuged. The precipitate was washed with 1 L of a 1:10 HCl solution, and then dialyzed for a week to remove acids and ions.

Synthesis of CoS/rGO composite

80 mg of the as-prepared GO was dispersed into 70 mL of DI water under ultrasound for 4 h to form a uniform dispersion. Then, 1 mmol of $CoCl_2 \cdot 6H_2O$ was added into the above dispersion under stirring, followed by adding 0.5 mmol of $Na_2S_2O_3 \cdot 5H_2O$. After stirred for 0.5 h, the mixture was added with 2 mL of hydrazine hydrate, transferred into a 100 mL of Teflon-lined autoclave and then heated at 180℃ for 12 h. The produced CoS/rGO was centrifuged, washed with DI water and ethanol each for several times and dried in a vacuum oven at 60 ℃. CoS was also prepared by using the same method without GO as a comparison.

Material Characterizations

X-ray diffraction (XRD) patterns were acquired with an XRD-6000 instrument (Shimadzu, Japan) with a Cu Kα radiation source. Fourier transform infrared (FTIR) spectra were recorded with a Bruker VECTOR22 spectrometer. Morphologies of the samples were observed by scanning electron microscopy (SEM, Hitachi S-4800) with an energy dispersive X-ray spectrometer (EDS), and transmission electron microscope (TEM, JEOL2010). Raman spectra were obtained with a Horiba Jobin-Yvon Raman spectrometer with a 532.0 nm excitation wavelength from an argon ion laser source with an output power of 0.02 mW. The Brunauere-Emmette-Teller (BET) surface area and pore size distribution (PSD) were measured with the equipment of ASAP 2020. The electrical conductivity of samples was measured at room temperature by a four-point probe method (RTS-8 4-point probes resistivity measurement system, Probes Tech., China).

Electrochemical Measurements

The electrochemical measurements were carried out in a 6 mol/L of KOH electrolyte with a three-electrode configuration where a platinum and a saturated calomel electrode were served as the counter and the reference electrode, respectively. The working electrode was prepared by mixing 80 wt% of the composite, 10 wt% of carbon black and 10 wt% of a nafion solution and dropping them onto a carbon electrode with a diameter of 1 cm, having 1 mg of the active materials. A two-electrode symmetry configuration was set up by using two above as-prepared electrodes with a center distance of 15 mm without counter electrode and reference electrode. Cyclic voltammetry (CV) measurements, galvanostatic charge-discharge tests and electrochemical impedance spectroscopy (EIS) tests were performed on a CHI 600 electrochemical workstation at room temperature.

Results and discussion

Here we used sodium thiosulfate as a sulfur source rather than thiourea and thioacetamide, mainly considering its lower cost and easier acquirementv, which is important in practical use. When $CoCl_2$ was added into the GO suspension, the Co^{2+} could react with the oxygen group on GO by the electrostatic attraction and be anchored on the GO sheets. In the presence of hydrazine hydrate and sulfur source, the reduction from GO to rGO and the generation of CoS crystals on rGO sheets could be achieved simultaneously during the hydrothermal process. During this reaction process, the hydrazine hydrate could product gases such as NH_3 and N_2,

which was beneficial to form a porous structure of the materials. The reaction could be briefly described as:

$$N_2H_4 + Co^{2+} + S_2O_3^{2-} + GO \rightarrow CoS + rGO + NH_3 + N_2$$

Figure 1a shows the EDS spectrum of the CoS/rGO composite, which confirmed that the composite was composed of C, O, S and Co. The Si element arised from a Si substrate. The molar ratio of Co to S was around 1:1, revealing the existence of CoS in the composite. The small peak relating to O element implied the presence of trace oxygen-containing groups, which may contribute capacitance of the composite material but the impact may be slight [28, 29]. Figure 1b shows the XRD patterns of the CoS/rGO composite, GO, rGO and CoS. It can been seen that the composite shows a broad peak centered at 24°, belonging to the disordered stacking of rGO sheets [30], and the absence of a peak at 10.6 °, which attributed to [001] face of GO [31], confirms that GO has been reduced to rGO. Comparing with the pattern of bare CoS, the peaks at 30.7, 36.0, 47.5, and 54.2 attributed to [100], [101], [102], and [110] faces of CoS (JCPDS No. 65-3418, hexagonal phase) become weaker in intensity and broader in width, suggesting the composite has a lower crystallinity. Figure 1c shows Raman spectra of the composite and GO. Each pattern had two peaks at about 1350 cm^{-1} and 1580 cm^{-1} corresponding to a disordered (D) carbon and graphitic (G) carbon structure respectively [32]. The larger D/G intensity ratio of the CoS/rGO composite than the bare GO implied more disordered carbon structure of CoS/rGO and the reduction of GO, which was consistent with the XRD results. Figure 1d gives an XPS spectrum of the composite. The detected elements C, O, Co and S are the

same as the result from the EDS, verifying further the structure of the composite. The S 2p peak at 159.2 eV and the Co 2p peak at 780.0 eV are the characteristics of cobalt sulfide [33]. The C 1s peak at 284.2 eV is from the carbon of rGO and the O 1s peak at 532.0 eV indicates the presence of residual oxygen containing groups. Besides, the spectrum of Co 2p reveals the Co^{2+} in the composite. Based on all above analysis, we believe that the CoS/rGO composite was successfully prepared with a clear composition.

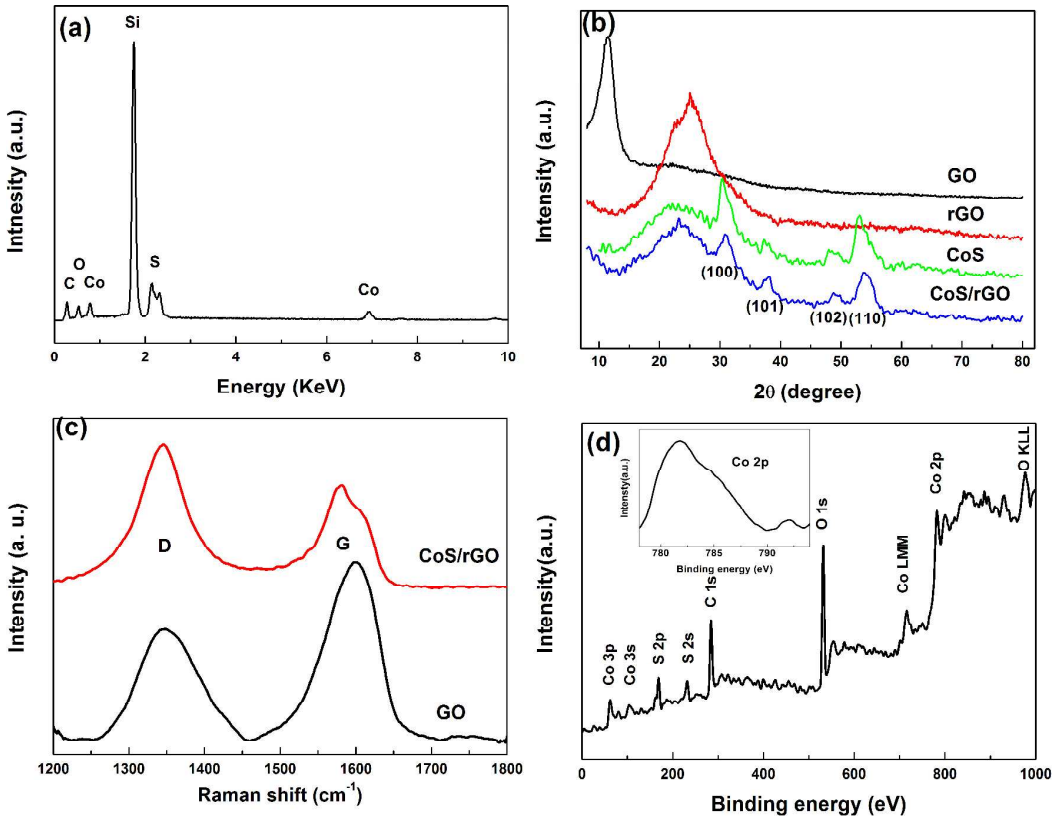

Figure.1. (a) EDS pattern of CoS/rGO; (b) XRD patterns of CoS, GO, rGO and CoS/rGO; (c) Raman spectra of GO and CoS/rGO; (d) XPS survey spectrum of the composite and the magnified Co 2p peak.

To further understand the percentage of CoS and rGO, TGA measurement of the CoS/rGO composites was taken from room temperature to 800℃ in air. By analyzing the curve in Figure 2a, the weight loss from 500℃ to 650℃ is due to the burning of bare graphene sheets [1], suggesting that the weight percentages of CoS and rGO in the CoS/rGO composite were about 62 wt% and 38 wt% respectively. The specific surface area of the composite measured based on the BET method was calculated to be 33.6 m^2/g, which is offered from majority of the pores about 3.43 nm and a few pores of 10.34 nm, as shown in Figure 2b. All these pores are mesopores and could serve as channels for the rapid transport of ions [17]. So, in our case, the measured specific surface area is equivalent to nearly the actual effective surface area, thus endowing the composites a high electrochemical performance.

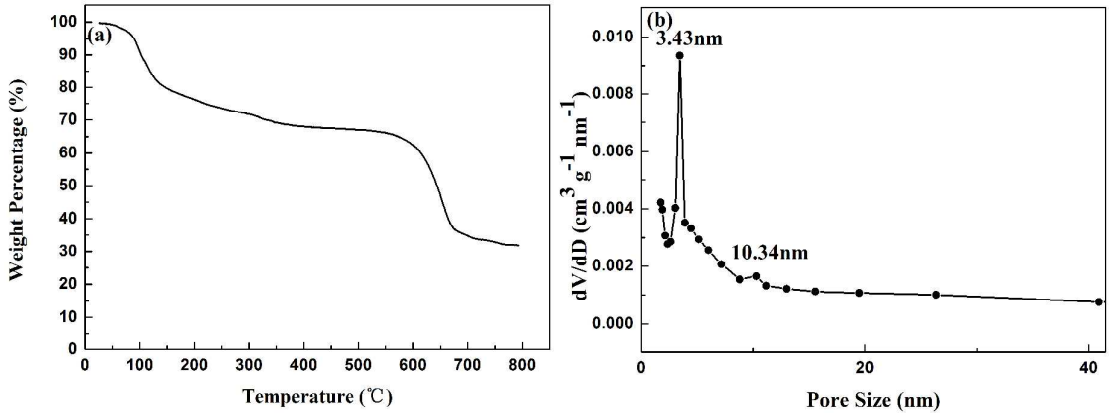

Figure.2. (a) TGA curves of CoS/rGO in air ranging from room temperature to 800℃; (b) pore size distribution of the CoS/rGO composites.

The microstructure of the CoS/rGO composite is characterized further by SEM and TEM (Figure 3). Comparing with the CoS irregular particles (Figure 3a), the CoS/rGO composites showed a composite structure, in which the CoS particles with a

size about 200-400 nm were distributed on the surface of the rGO nanosheets (Figure 3b and 3c). The HRTEM image of CoS particles on the composite (Figure 3d) displayed a fringe spacing of 0.291 nm, which is corresponding to the (100) phase of CoS.

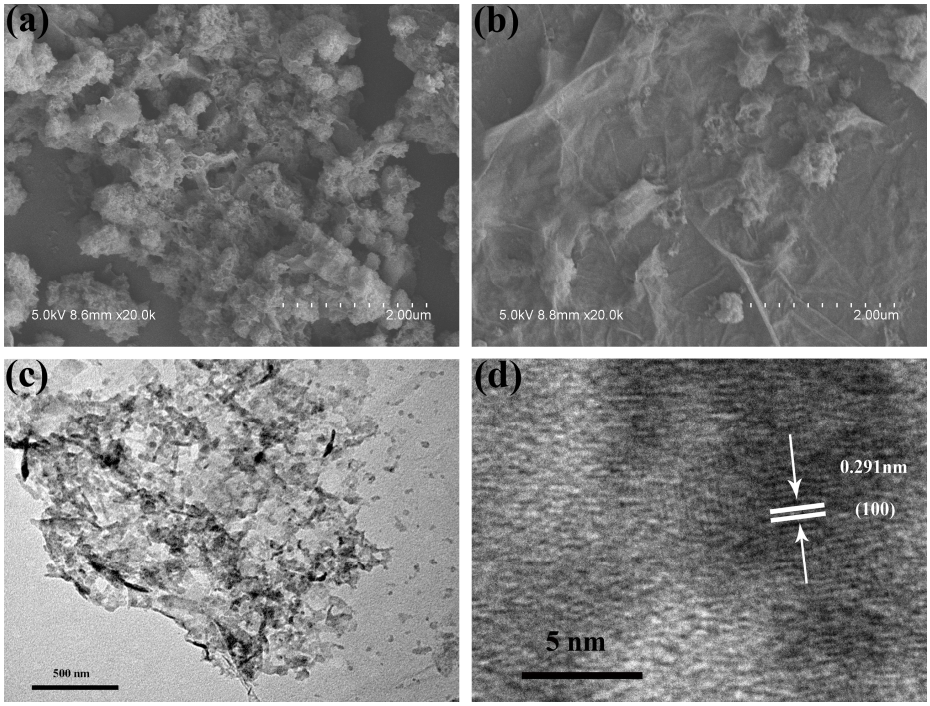

Figure.3. (a) SEM image of the bare CoS; (b) SEM image of the CoS/rGO composite; (c) TEM image of the CoS/rGO composite;(d) high resolution TEM image of the CoS/rGO composite.

To evaluate the CoS/rGO composite as an electrode material of a supercapacitor, several electrochemical tests were carried out with a three-electrode configuration. Figure 4a and 4b displayed the CV profiles of the bare CoS and the CoS/rGO composite in 6 M of KOH aqueous solution at various scan rates. Two possible electrochemical reactions during the measuring process are proposed [34].

$$CoS + OH^- \leftrightarrow CoSOH + H_2O + e^-$$

$$CoSOH + OH^- \leftrightarrow CoSO + H_2O + e^-$$

In contrast with bare CoS, the composite exhibited a more rectangular curve due to the presence of rGO, indicating its better reversibility and electrochemical performance. It can be noted from the CV curves that the specific capacitance of CoS/rGO electrode is much higher than that of the bare CoS electrode, suggesting that with the presence of rGO, the composite shows much better electrochemical property. Figure 4c shows the galvanostatic charge-discharge profiles of the CoS/rGO composite electrode in 6 M of KOH at various current densities from 1 A/g to 40 A/g. The values of specific capacitance were calculated based on the discharge stages of the electrodes by applying the following equation: $C = It/m\Delta V$, where I represents a constant current applied to the charge-discharge process, m is a mass of an active material on a electrode, t is time consumed for a discharge process, and ΔV is a potential window. The composite electrode shows reversible charge-discharge cycles and the specific capacitances of 550, 538, 522, 468, and 400 F/g at the current densities of 1, 5, 10, 20, and 40 A/g, respectively, revealing its high specific capacitance and good rate capability. When the current density raises to 10 A/g from 1 A/g, the specific capacitance can remain 94.91 %; even as the current density raises as high as 40 A/g, the specific capacitance can still remain 72.73 %, which is much higher than many reported results with nearly the same active electrode materials[1, 20, 35]. Figure 4d shows the specific capacitance of bare rGO, CoS and CoS/rGO composites measured at different current density. It can be seen that the composites

exhibit a much higher capacitance than bare CoS and rGO, which could be owed to the symergistic effect between CoS and rGO, that is, the anchored CoS particles on rGO sheets can prevent effectively the aggregation and restacking of rGO sheets thus inducing porosity and increasing the accessible surface of rGO nanosheets, which can facilitate greatly the ion diffusions. At the same time, combining CoS with rGO can provide extra pseudocapacitance, which makes the composite has the enhanced electrochemical performance.

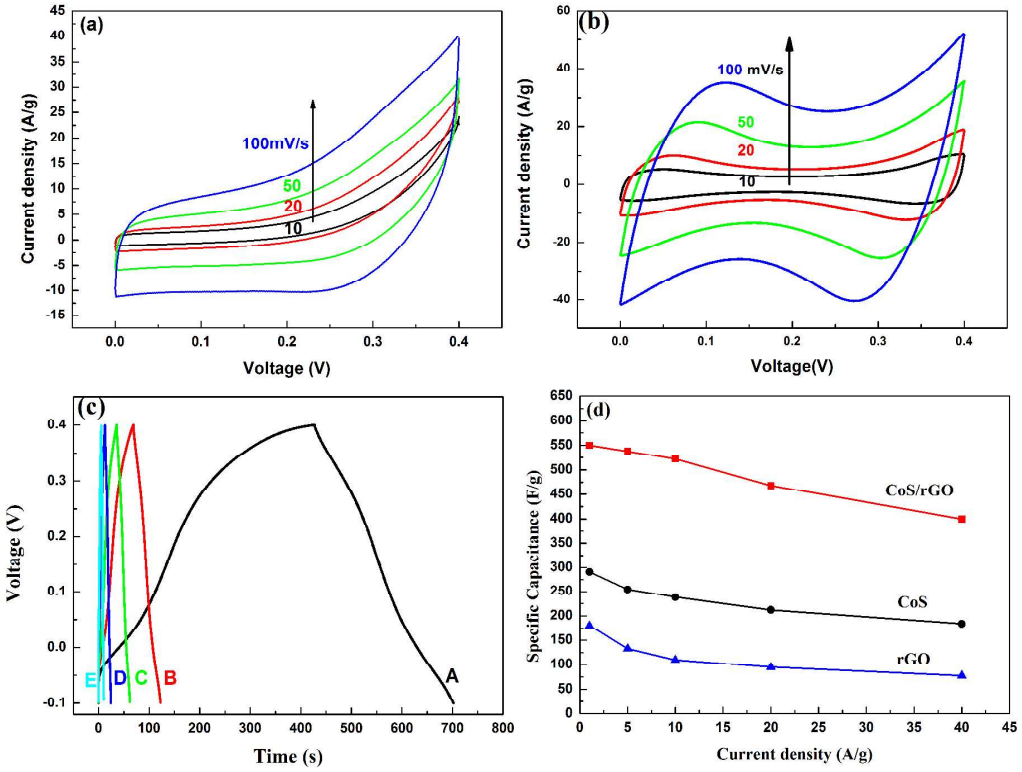

Figure.4. CV curves of (a) bare CoS and (b) CoS/rGO composite at various scan rates with a three-electrode configuration; (c) galvanostatic charge and discharge curves of CoS/rGO composite at a current density of (A) 1, (B) 5, (C) 10, (D) 20, (E) 40 A/g with a three-electrode configuration; (d) specific capacitances of CoS, rGO and the

CoS/rGO composite at various discharge current densities with a three-electrode configuration.

The galvanostatic charge-discharge cyclic stability curve of the CoS/rGO electrode is investigated at 5 A/g in a 6 mol/L of KOH aqueous solution. Figure 5a reveals the specific capacitance of the composite through 5000 cycles. It is seen that during the first 1000 cycles, the specific capacitance is maintained for 95 % (462.5 F/g), without noticeable decrease. After extended cycling for another 4000 cycles, around 90 % of the specific capacitance still can be maintained (437.5 F/g), evidently indicating the high cycling stability of the composite. This is mainly attributed to the favorable stability of the graphene. Besides that, the high rate capability and improved cycling stability of the composite could come from its low resistance revealed by EIS spectrum. As shown in Figure 5b, the CoS/rGO composite exhibited a smaller semi-circle in the high frequency and a more vertical line in the low frequency than the bare CoS, implying its lower interfacial charge-transfer resistance and better capacitive behavior with the ion diffusion transport. The measured conductivity data indicated that the CoS/rGO composite had a remarkably enhanced conductivity of 4.8 $\times 10^{-2}$ S/cm comparing to the bare CoS (5.56×10^{-5} S/cm) due to the presence of rGO,

which is consistent with its internal resistance shown in Figure 5b[36].

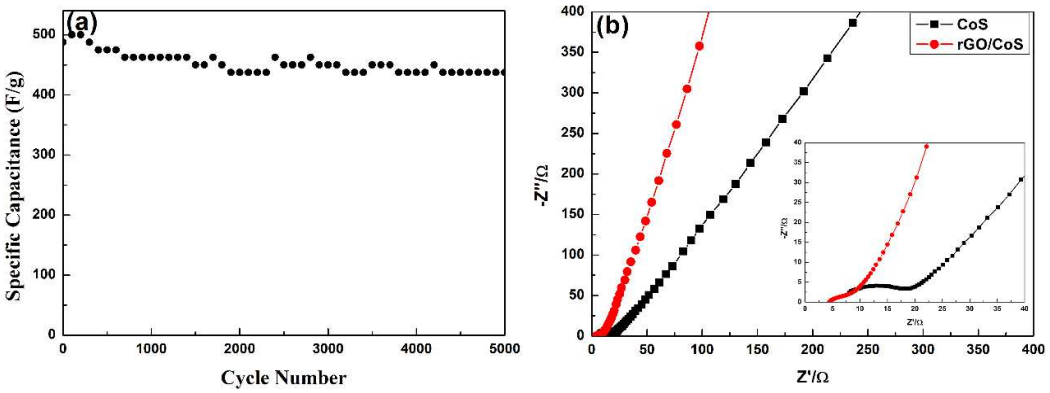

Figure.5. (a) Cycling performance of CoS/rGO at 5A/g for 5000cycles; (b) Impedance Nyquist plots of CoS and CoS/rGO composites.

Figure 6b shows the Ragone plot (energy density vs. power density) of the CoS/rGO composite depends on the specific capacitances (Figure 6a) obtained from a two-electrode system. Energy density (E) and power density (P) are normally used as important parameters to characterize and assess an electrochemical performance of a supercapacitor. They can be obtained from a galvanostatic charge/discharge test by varying current densities and calculated by the formulas of $E=C_s(\Delta V)^2/2$ and $P=E/\Delta t$, where C_s is a capacitance of a two-electrode capacitor, ΔV is a voltage decrease during discharge and Δt is time consumed during discharge. As seen from the Ragone plots, compared to the energy density decreased from 30.2 W h kg^{-1} to 13.6 W h kg^{-1}, the power density can even increase from 1.4 kW kg^{-1} to 24.5 kW kg^{-1}. E and P in this study were pretty high and larger than those of some carbon-based capacitors [37, 38].

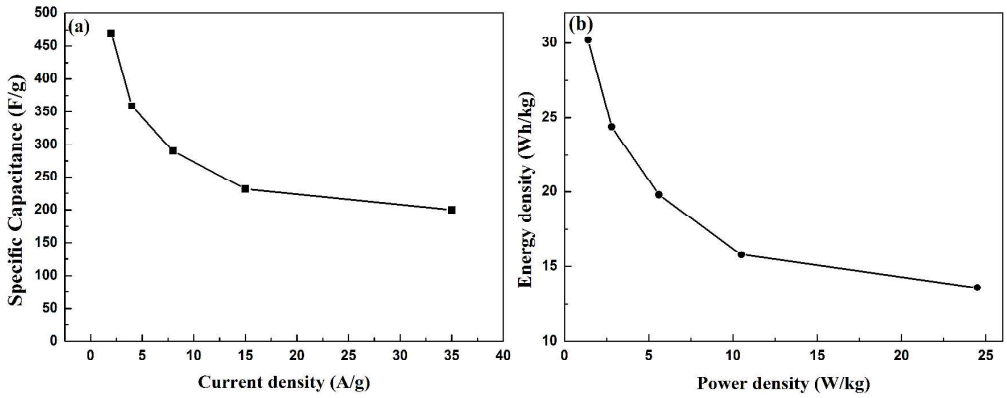

Figure.6. (a) specific capacitances of the CoS/rGO composite at various discharge current densities with a two-electrode configuration. (b) Ragone plot (energy density vs. power density) of the CoS/rGO composite electrode at various charge-discharge rates with a two electrode system.

We hypothsize that the superior electrochemical performance of this CoS/rGO composite was attributed to the following reasons: 1) the high conductivity and electrochemical stability of rGO nanosheets could facilitate the electron transport during the charge-discharge process; 2) CoS particles anchored on the rGO surface could prevent the aggregation and restacking of rGO sheets, forming a stable structure and thus enabling the composite a long cyclic life; 3) the specific surface area (33.6 m^2/g) and the abundant tiny pores of about 3 nm were beneficial for the contact of electrolytes with the electrode material, shortening the diffusion path of electrolyte ions.

Conclusion

We have successfully prepared the CoS/rGO composite with a simple and one-step hydrothermal method. The CoS particles were about 200-400 nm and anchored uniformly on the surface of rGO. The CoS/rGO composite was applied as an electrode for a supercapacitor, which provided a high specific capacitance of 520 F/g at a current density of 1 A/g, and brought 400 F/g with an even much higher current density of 40 A/g. These high specific capacitances revealed an extraordinary rate capability. The CoS/rGO electrode also showed a high cyclic stability. The specific capacitance still can remain 90 % after 5000 cycles of charge/discharge. Besides, the composite electrode showed pretty high energy density as well as power density. These excellent electrochemical performance of the CoS/rGO composite could be attributed to the introduction of graphene, which provided high electrical conductivity and electrochemical stability. CoS/rGO composite could be a promising electrode material for a high performance supercapacitor.

Acknowledgement

This work was supported by the National Natural Science Foundation of China (No. 21174059, 21374046), Program for Changjiang Scholars and Innovative Research Team in University, Open Project of State Key Laboratory of Superamolecular Structure and Materials (SKLSSM2015015) and the Testing Foundation of Nanjing University.

References

1 B. Wang, G. Park, D.W. Su, C.Y. Wang, H.J. Ahn, G.X. Wang. *J. Mater. Chem*, 2012, **22**, 15750-15756.

2 L. Qian, X.Q Tian, L. Yang, J.F. Mao, H.Y. Yuan, D. Xiao. *RSC Adv.*, 2013, **3**, 1703-1708.

3 G.F. Ma, H. Peng, J.J Mu, H.H. Huang, X.Z. Zhou, Z.Q. Lei. *J. Power Sources*, 2013, **229**, 72-78.

4 T. Zhu, Z.Y Wang, S.J. Ding, J.S. Chen, X.W. Lou. *RSC Adv*., 2011, **1**, 397-400.

5 H.L. Wang, Y.Y. Liang, Y.G. Li, H.J. Dai. *Angew. Chem. Int. Ed.*, 2011, **50**, 10969-10972.

[6] R.C. Hoodless, R.B. Moyes, P.B. Wells. *Catal Today*, 2006, **114**, 377-382.

[7] Y. Kim, J.B. Goodenough JB. *J. Phys. Chem. C.*, 2008, **112**, 15060-15064.

[8] P.J. Masset, R.A. Guidotti. *J. Power Sources,* 2008, **178**, 456-466.

[9] Q.H. Wang, L.F. Jiao, H.M. Du, J.Q. Yang, Q.N., Huan, W.X. Peng, Y.C. Si, Y.J. Wang, H.T. Yuan. *CrystEngComm*, 2011, **13**, 6960-6963.

[10] W.J. Dong, X.B. Wang, B.J. Li, L.N. Wang, B.Y. Chen, C.R. Li, X. Li, T.R. Zhang, Z. Shi. *Dalton Trans.,* 2011, **40**, 243-248.

[11] Y.X. Zhou, H.B. Yao, Y. Wang, H.L. Liu, M.R. Gao, P.K. Shen, S.H. Yu. *Chem. Eur. J,* 2010, **16**, 12000-12007.

[12] Q.H. Wang, L.F. Jiao, Y. Han. *J. Phys. Chem. C.*, 2011, **115**, 8300-8304.

[13] R.L. Tseng, S.K. Tseng. *J. Colloid. Interface. Sci.*, 2005, **287**, 428–437.

[14] R. Zhang, W. Li, X.Y. Liang, G.P. Wu, Y.G. Lu, L. Zhan, C.X. Lu, L.C. Ling. *Micropor Mesopor Mat*, 2003, **62**, 17-27.

[15] P. Liu, Y. Wei, L. Liu, K.L. Jiang, S.S. Fan. *Nano Res*, 2012, **6**, 421-426.

[16] C. Merino, P. Soto, E. Vilaplana-Ortego, J.M. Gomez, F. Pico, J.M. Rojo. *Carbon*, 2005, **43**, 551–557.

[17] D.W. Wang, F. Li, M. Liu, G.Q. Lu, H.M. Cheng. *Angew. Chem. Int. Ed.*, 2008, **47**, 373–376.

[18] A.K. Geim, K.S. Noveselov. *Nature Mater*, 2007, **6**, 183-191.

[19] A.H. Castro Neto, F. Guinea, NMR. Peres. *Rev. Mod. Phys.*, 2009, **81**, 109-162.

[20] B.H. Qu, Y.J. Chen, M. Zhang, L.L. Hu, D.N. Lei, B.G. Lu, Q.H. Li, Y.G. Wang, L.B. Chen, T.H. Wang. *Nanoscale*, 2012, **4**, 7810-7816.

[21] Q. Pan, J. Xie, S.Y. Liu, G.S. Cao, T.J. Zhu, X.B. Zhao. *RSC Adv.*, 2013, **3**, 3899-3906.

[22] K. Chang, W.X. Chen. *ACS Nano*, 2011, **5**, 4720-4728.

[23] K. Chang, W.X. Chen. *Chem. Commun.*, 2011, **47**, 4252-4254.

[24] G.C. Huang, T. Chen, Z. Wang, K. Chang, W.X. Chen. *J. Power Sources*, 2013, **235**, 122-128.

[25] H.Z. Wan, J.J. Jiang, J.W. Yu, Y.J. Ruan, L. Peng, L. Zhang, H.C. Chen, S.W. Bie. *Appl. Sur. Sci.*, 2014, **311**, 793-798.

[26] Y. Wang, J. Tang, B. Kong, D.S. Jia, Y.H. Wang, T. An, L.J. Zhang, G.F. Zheng. *RSC Adv.*, 2015, **5**, 6886-6891.

[27] N.I. Kovtyukhova, P.J. Ollivier, B.R. Martin, T.E. Mallouk, S.A. Chizhik, E.V. Buzaneva, A.D. Gorchinskiy. *Chem. Mater.*, 1999, **11**, 771-778.

[28] C.T. Hsieh, W.Y. Chen, Y.S. Cheng. *Electrochim. Acta*, 2010, **55**, 5294-5300.

29 C.T. Haieh, S.M. Hsu, J.Y. Lin H. Teng. *J. Phys. Chem. C.*, 2011, **115**, 12367-12374.

[30] J.Q. Tian, H.Y. Li, Z.C. Xing, L. Wang, Y.L. Luo, A.M. Asiri, A.O. Al-Youbi, X.P. Sun. *Catal. Sci. Technol.*, 2012, **2**, 2227-2230.

[31] K. Zhang, L.L. Zhang, X.S. Zhao, J.S. Wu. *Chem. Mater.*, 2010, **22**, 1392-1401.

[32] F. Uinstra, J.L. Koenig. J. *Chem. Phys.*, 1970, **53,** 1126–1130.

[33] S.J. Bao, Y.B. Li, C.M. Li. *Cryst. Growth Des*, 2008, **8**, 3745-3749.

[34] C.Y. Chen, Z.Y. Shih, Z. Yang, H.T. Chang. *J. Power Sources*, 2012, **215**, 43-47.

[35] Q.H. Wang, L.F. Jiao, H.M. Du, Y.C. Si, Y.J. Wang, H.T. Yuan. *J. Matter. Chem.*, 2012, **22**, 21387-21391.

[36] C.Q. Shang, S.M. Dong, S. Wang, D.D. Xiao, P.X. Han, X.G. Wang, L. Gu, G.L. Cui. *ACS Nano*, 2013, **7**, 5430-5436.

[37] Y. Wang, Z.Q. Shi, Y. Huang. *J. Phys. Chem. C.*, 2009, **113**, 13103–13107.

[38] A.T. Chidembo, K.I. Ozoemena, B.O. Agboola, V. Gupta, G.G. Wildgoose, R.G. Compton. *Energy Environ*. Sci., 2010, **3**, 228–236.

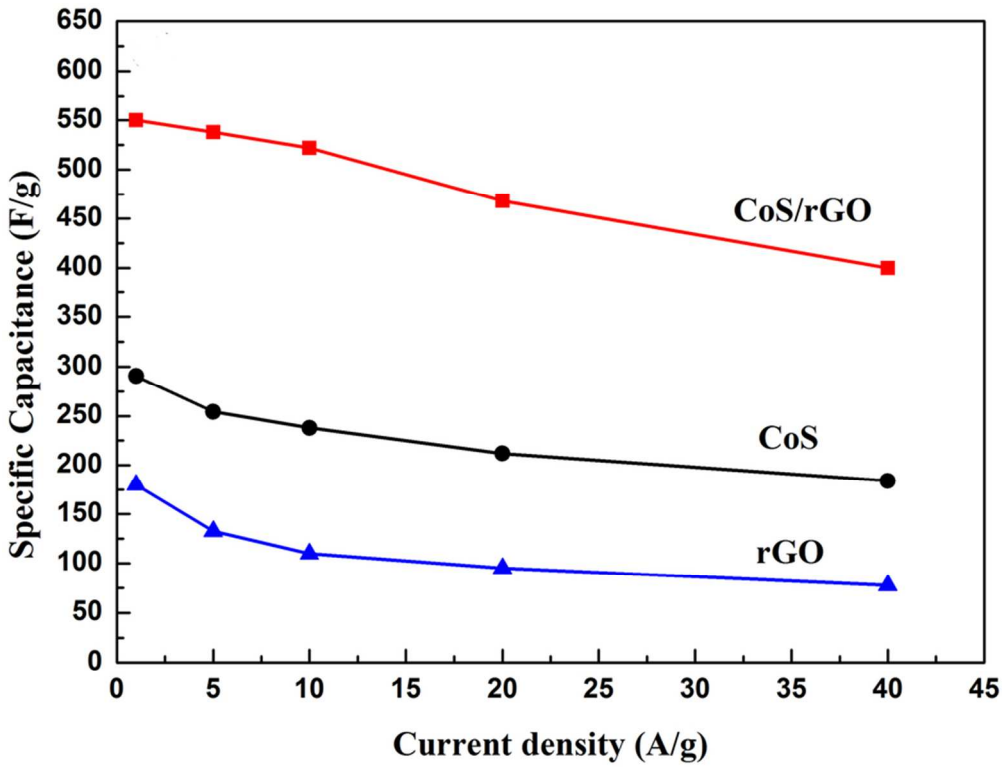

The CoS/rGO composite electrode exhibit a rather high rate capability.
39x30mm (600 x 600 DPI)